Desalination and Water Treatment
www.deswater.com

doi: 10.5004/dwt.2019.23589

143 (2019) 137–147
March

Hydraulic design perspectives of bioswale vegetation layers: a meta-research theory

Joshua Lelemia Irvine, Albert S. Kim*

Department of Civil and Environmental Engineering, University of Hawaii at Manoa, 2540 Dole Street, Holmes Hall 383, Honolulu, Hawaii 96822, USA, Tel. +1 808 956 3718; Fax: +1 808 956 5014; emails: albertsk@hawaii.edu (A.S. Kim), joshuair@hawaii.edu (J.L. Irvine)

Received 9 October 2018; Accepted 7 November 2018

ABSTRACT

Optimized bioswale-design requires a fundamental understanding of mass and momentum transfer through a bioswale vegetation layer (BVL) on top of the porous soil zone. Conventional theories of canopy flows are applicable to structuring BVL in a planning phase. Plants in the BVL can be modeled as an embedded collection of cylindrical rods characterized by using (mean) diameter and height. The number density and spatial periodicity of the plants determine the structural and hydraulic characteristics of the BVL. The current paper stands as what we are calling meta-research or "research of research" consisting of an in-depth literature review followed by our own theoretical development and its application. A design equation for an emergent BVL is developed, which suggests the minimum length-to-width ratio of a bioswale as a function of runoff hydraulic characteristics. We calculate a proper bioswale length near which the viscous force fully supersedes the inertial force along the BVL. Moreover, a supplementary graphical method is developed within this study as a simple tool with which to design bioswale dimensions.

Keywords: Bioswale vegetation layer (BVL); Bioswale design equations; Canopy-flow theory; Runoff Reynolds number; Stormwater management; Plant density

1. Introduction

A bioswale exists as a nature-based infrastructure, widely used for low-impact development (LID) in modern urban environments, which was first practiced in Prince George's County, Maryland, in the early 1990s [1–3] to reduce stormwater runoff and remove non-point source pollutants [4–6]. A typical bioswale structure has dual or stratified layers, consisting of overland vegetation and engineered soil zones. The underground soil zone is often pictured as a porous media of varying porosity and hydraulic conductivity. Physico-chemical characteristics of the porous media determine the runoff and pollutant removal capacities [7,8]. As current bioswale designs depend on empirical guidelines and suggestions, systematic research on bioswale transport phenomena began only recently [9].

Structural modifications of LID systems are challenging in a practical sense after their initial installation due to their large size and initial costs. The estimation of the bioswale life-expectancy is, therefore, an important process to ensure long-term operations, possibly with minimum maintenance. Within the existing literature, bioswale research has been focused primarily on experimental observations of runoff infiltration and pollutant removal within the underground soil media by measuring input and output flow rates and concentrations. The top surface of a bioswale is often covered with a bioswale vegetation layer (BVL) primarily for landscaping purposes. The BVL possesses structural as well as

* Corresponding author.

hydraulic aspects, which need to be considered for geometrical designs because the BVL controls the longitudinal flow field and pressure distribution upon the permeable bioswale surface. To the best of our knowledge, engineering roles of the BVL have not been actively studied.

The basic fluid mechanics research on canopy flow can be readily employed to investigate the BVL for the proper management of inland, overland, and infiltrating runoff flows. As the runoff infiltration followed by the pollutant removal depends on the hydraulic drag created in the BVL, a proper design of the BVL is as important as that of the internal porous structure of the bioswale. In this work, we first examine the applicability of canopy-flow theories correspondingly to the BVL analysis. Second, we derive a new design equation for proper bioswale sizing. And, third, we develop a comprehensive graphical method that visually links hydraulic aspects of runoff flows and geometrical aspects of the BVL structures. To explain the coupled role of the BVL, we include a brief research background and a theoretical review in the following sections and propose a practical graphical method as a BVL sizing tool.

2. Background

2.1 Particle and pollutant removal

A standard bioswale controls pollutant and solid loads from a surrounding catchment area [10]. Bäckström [11,12] monitored the hydrological performance of a bioswale system over a 12-month period and found that total suspended solids (TSS) removal had been reduced by 99% along a 100 m bioswale. Achleitner et al. [13] investigated bioswales ranging from 2 to 10 years of age and reported that regulatory assumption of 15 years is a reasonable estimation of the replacement time of the engineered soil media [13]. Roinas et al. [14] observed that most TSS removal occurs near an inlet bioswale zone. Xiao and McPherson measured inlet and outlet concentration of suspended solids through a bioswale installed in a parking lot and reported 95% of removal by measuring inlet and outlet concentrations [15]. Trowsdale and Simcock [16] also examined the TSS removal capability of a bioretention system, and found that the median concentrations of zinc retained in the bioswale system still exceeded ecosystem health guidelines. Other studies focused on hydraulic and hydrologic aspects of bioswales through field studies [16,17] and lab-scale experiments [18,19]. Even though the aforementioned studies provide engineering insights regarding the removal capability of bioswales, these empirical analyses are limited to a small number of detection points, asynchronized measurements with long time intervals, and visual investigation subject to human perspectives. Moreover, coupled effects of surface runoff, the BVL structures, and pollutant/solid removal were not systematically studied.

2.2. Design methods

Design methods based on empirical correlations or instructional criteria often indicate the minimum regulatory requirements so as to build bioretention systems [20–23]. These guidelines, however, do not provide thorough methods based on scientific rigor in order to address site-specific optimization of a bioswale. Based on our analysis of the stormwater guidelines for the western United States, five approaches exist for sizing bioswales, which include Darcy's law [24,25], the rational method [26–28], Manning's equation [29], the curve number method [30], and the first-flush sizing method [31]. In reality, bioswales can have various topologies of surrounding ground surfaces, where the runoff flows are conveyed toward bioswale inlets. Although a rigorous computational method such as computational fluid dynamics can be used, there still exists a strong need to have improved design equations for the bioswale sizing.

2.3. Plant structure

Conventional models for canopy flows have described vegetation structures as rigid or flexible stems in either submerged or emergent conditions, where the physical stem height is lower and higher than flowing water height, respectively. Originally, Petryk [32] experimentally investigated flows passing a group of submerged cylinders in an open channel and developed a model to correlate the mean velocity distribution across the channel, the drag forces upon each cylinder, and the hydraulic resistance among a group of cylinders. This model is, however, limited to uniform laminar flow in a sparse stem configuration for subcritical Reynolds numbers, for which the spacing between the nearest cylinders are at least six stem diameters in the downstream direction. In the past decades, various researchers investigated the effect of vegetation configurations on its overall hydraulic resistance to incoming runoff flows [32–38].

2.4. Hydraulic/hydrologic aspects

The hydraulic/hydrologic aspects of a canopy layer research can be briefly summarized as follows. For an emergent and flexible vegetation, Fathi-Maghadam and Kouwen [39] developed a mathematical model to estimate Manning's roughness coefficient of flexible, emergent vegetative layers. Finnigan [40] developed a heuristic model, which provides an innovative perspective on turbulence flow passing planted canopies for both the submerged and emergent cases. This model qualitatively describes the three development stages of the mixing boundary layer within vegetation zones of various porosities. The stages include (1) the emergence of the primary Kelvin–Helmholtz instability, (2) the clumping of the vorticity of the Kelvin–Helmholtz waves into vortices, and (3) the kinking and pairing of the vortices. Despite the ecological and engineered significance of hydraulic interactions between vegetation layers and interstitial fluid flows, there is a paucity of studies that have examined the influences of canopy/bioswale structures on the hydraulic drag to the interstitial flow fields. The direct numerical simulation method was used to examine single-particle capture by a circular cylinder in vortex-shedding regimes [41–43]. Although the work of Espinosa-Gayosso et al. [41–43] accurately simulated low-Reynolds number flows, their respective system includes only a pair consisting of a particle and an embedded cylinder so that the many-body hydrodynamics was not included. King et al. [44] characterized the aquatic vegetation as rigid cylinders fixed upon an impermeable ground surface so as to model flow in the vegetation layer. They conducted physical experiments to validate their turbulence model through emergent and submerged

BVL cases. Although the experimental validation was successful within their study, six parameters should be calibrated in addition to the standard $k - \epsilon$ model coefficients: flow depth, vegetative height, drag coefficient, volume fraction, projected plant area per volume, and stem diameter. Existing canopy-flow models are readily applicable to the BVL investigation using the stem-cylinder analogy [45–47].

As discussed previously, bioswale systems provide an important transition zone from impervious artificial surfaces to porous natural ground. Thus, understanding a bioswale's hydrodynamic response to incoming runoff flow is a critical procedure in order to characterize the respective bioswale structure.

3. Theoretical review

An understanding of flow resistance and conveyance capacity is critical for hydraulic BVL characterization. Vegetation arrays (i.e., geometrical obstacles) can be described as either submerged or emergent conditions, which may dynamically change with time during a precipitation event depending on the runoff height. The obstacles create a specific hydraulic drag that resists the incoming flow to the internal BVL region. The drag coefficient of a canopy medium can be defined as:

$$C_D = \frac{F_D / A_c}{\frac{1}{2}\rho V^2} = \frac{\text{Dissipated energy density}}{\text{Kinetic energy density}} \tag{1}$$

where F_D is the average drag force along the direction of the average flow, A_c is the area of the plant array, ρ is the fluid density, and V is a representative fluid velocity.

Fig. 1 shows the geometrical aspect of stems embedded within the bioswale surfaces, in which (a) and (b) indicate the submerged [48–50] and emergent conditions [51–56], respectively, and (c) and (d) show staggered [38,57] and squared [38,50] configurations of embedded stems, respectively. The submerged phase indicates that the dynamic water height h_w is higher than the physical plant height h_v, which is equal to the wetted plant height l, that is, $h_w > h_v$ and $l = h_v$. The emergent phase is characterized using $h_w < h_v$ and $l = h_w$. Mathematically, the wetted length can be expressed as follows:

$$l = \min\left(h_w, h_v\right) \tag{2}$$

which means l is the shorter one between h_w and h_v. Runoff flows entering the bioswale generally have a transient water height due to transient precipitation patterns. The BVL would, therefore, dynamically experience both emergent and submerged conditions. In particular, if a BVL exists as a short grass layer, then the role of the grasses can be better viewed as a non-smooth surface with a specific roughness providing a slip boundary condition. On the other hand, if the BVL consists of plants of an order of $O(10)$ cm, the emergent phase is preceded before reaching the submerged phase. In this light, we briefly discuss standard theories of canopy flows as applicable to the bioswale sizing.

3.1. Submerged canopy theories

3.1.1. Barfield et al.'s work

Barfield et al. [58] developed the general shear stress model for the submerged condition by defining a spacing hydraulic radius

$$r_{\text{BTH}} = h_v \left(\hat{h}_w - 1 + \frac{\hat{s}}{2 + \hat{s}} \right) \tag{3}$$

and the ratio between bed and total shear stresses

$$f_{\text{BTH}} = 1 - \left(\hat{h}_w + \frac{1}{2} \hat{s} \hat{h}_w \right)^{-1} \tag{4}$$

where $\hat{h}_w = h_w/h_v$ and $\hat{s} = s/h_v$ are normalized lengths of water and stem-spacing by the plant length h_v, respectively, s is the spacing of the elements in the vegetation canopy, and the subscript BTH indicates the three authors of the work [58]. Without losing the generality, Eqs. (3) and (4) can be applied for an emergent condition by mathematically letting $h_v = h_w$ and $h_v = l$ by considering hydraulic drags generated on the wetted surfaces. For the emergent case, a portion of a stem above the water level is assumed to have negligible contribution to the total hydraulic drag. Therefore, the physical length of the stem can be replaced by the wetted length l.

3.1.2. Stone and Shen's work

Stone and Shen [36] investigated a steady open-channel flow through submerged cylindrical stems of an equal height, distributed uniformly over a bed area. The total stress due to the water flow τ_w was represented as follows:

$$\tau_w = \tau_v + \tau_b \tag{5}$$

as a superposition of those due to the vegetation layer τ_v and the bed surface τ_b

$$\tau_w = \rho g S h_w \left(1 - \lambda \hat{l} \right) \tag{6}$$

$$\tau_v = \frac{1}{2} \rho C_D N d_s l V_c^2 \tag{7}$$

where g is the gravitational acceleration, S is the channel slope, d_s is the stem diameter, N is the number of plants per unit area, and $\hat{l} = l / h_w$ is the wetted height divided by the physical stem length. In Eq. (7), V_c is the maximum velocity within the vegetation layer, which is related to the approaching velocity V_l as follows:

$$V_l = V_c \left(1 - d\sqrt{N} \right) = V_c \left[1 - \sqrt{\frac{4\lambda}{\pi}} \right] \tag{8}$$

where the area concentration λ is defined as the fraction of the bed area occupied by cylindrical stems

$$\lambda = \frac{\pi d_s^2}{4} N = \frac{\pi}{4} a d_s \quad (9)$$

where $a = Nd_s$ is the projected plant area per volume. Then, the bed friction stress is derived as follows:

$$\tau_b = \frac{1}{8}\rho V_1^2 f_b (1-\lambda) = \frac{\rho g}{C_b^2} V_1^2 (1-\lambda) \quad (10)$$

where f_b represents the friction factor, and C_b is the Chézy coefficient of the channel bed [59]. Finally, the flow resistance R_{SS} is represented as follows:

$$R_{SS} = 1.385\left(\frac{1}{l} - \sqrt{d_s^2 N}\right)\sqrt{\frac{g}{N d_s h_w}} = 1.385\left(\frac{h_w}{l} - \sqrt{\frac{4\lambda}{\pi}}\right)\sqrt{\frac{\pi g d_s}{4\lambda h_w}} \quad (11)$$

of which the coefficient was obtained by a linear regression process using experimental data. In Eq. (11), we noticed a condition that R_{SS} is unconditionally positive, which derives an equivalent condition (i.e., $h_w \geq h_{onset}$), where

$$h_{onset} = \sqrt{N (d_s l)^2} \quad (12)$$

is an onset height of the water flow. Our interpretation of h_{onset} is as follows. If $h_w \leq h_{onset}$, then R_{SS} becomes negative, which is unphysical. A possible mathematical treatment is to replace Eq. (11) to

$$R_{SS} = \max(0, R_{SS}) \quad (13)$$

to replace a negative value of R_{SS} by 0. This mathematical trick physically implies that the hydraulic drag becomes meaningful if the water level is higher than the critical onset height h_{onset}.

3.1.3. Baptist's work

Baptist [60] proposed a resistance coefficient as follows:

$$R_B = \left(\frac{1}{C_b^2} + \frac{C_D a l}{2g}\right)^{-1/2} + \frac{\sqrt{g}}{\kappa}\ln\left(\frac{h_w}{h_v}\right) \quad (14)$$

where κ (=0.41) is the Von Karman's constant [61]. The bed shear stress is estimated as follows:

$$\tau_{bB} = \frac{\rho g}{C_b'^2}\bar{u}^2 \quad (15)$$

using a modified Chézy coefficient C'_b:

$$C_b' = C_b + \frac{\sqrt{g}}{\kappa}\ln\left(\frac{h_w}{h_v}\right)\sqrt{1 + \frac{C_D a h_v C_b^2}{2g}} \quad (16)$$

which is also applicable to emergent canopies by setting $h_w = h_v$.

3.1.4. Cheng's work

Cheng [50] developed a model to describe an effective resistance above and within the submerged vegetation layer in an open-channel flow. A vegetation-related hydraulic radius was defined in his work as follows:

$$r_v = \frac{\pi}{4}\frac{\lambda}{1-\lambda} D \quad (17)$$

and the global flow resistance is expressed as

$$R_{Ch} = (1-\lambda)\sqrt{\frac{2 g r_v}{l C_D}}\left(\frac{l}{h_w}\right)^{\frac{3}{2}} + 4.54\sqrt{g}\left[\left(\lambda^{-1}-1\right)\left(\frac{1 - l/h_w}{d_s/h_w}\right)\right]^{\frac{1}{16}}\left(1 - \frac{l}{h_w}\right)^{\frac{3}{2}} \quad (18)$$

by calculating the mean flow velocities within and above the vegetation layer. Note that the first and second terms of Eq. (18) has dependences on l/h_w and $1 - l/h_w$ with the same exponent of 3/2. In this case, the term of the squared bracket seems to be a pseudo-constant as its exponent is small (i.e., 1/16 = 0.0625 unless $d_s \ll h_w$).

3.1.5. Ghisalberti's work

Ghisalberti [62] developed a phenomenological model of obstructed flows across vegetation systems and investigated the vertical flow penetration from the top surface of the submerged obstruction layer of O(0.01 – 0.1 cm) height. As flow passes downstream through the obstruction zone, the hydraulic drag on the bottom surface initiates an upward flux above the vegetation layer. Ghisalberti [62] introduced a length scale of the vertical flow penetration, denoted as δ_e, and found that the $\delta_e C_D a \approx$ constant indicating that the length scale of the drag force is $(C_D a)^{-1}$. A higher drag C_D indicates a shorter penetration depth and lesser up-flow above the penetration zone. This penetration behavior was considered as a cause of vortex generation in the shear zone above the obstruction layer. Ghisalberti's findings can be summarized by $\omega_{\mathbf{rms}} \propto aU_h \propto u_{\mathbf{rms}} \propto u_*$, where ω_{rms} and u_{rms} are the vertical turbulent intensities at the interface and in the streamwise direction, respectively, u_* is the frictional velocity, and U_h is the slip velocity on the top of the obstruction layer.

3.2. Emergent canopy theories

Interestingly, the submerged canopy flows are investigated using flow resistance. In this section, emergent canopy theories are reviewed for the drag coefficient C_D.

3.2.1. Tanino et al.'s work

Tanino et al. [37] investigated the drag force exerted on randomly distributed, emergent circular cylinders of uniform diameter d, by using the dimensionless ratio of the mean viscous drag per unit cylinder, as originally proposed by Ergun [63] as:

$$\frac{\langle \overline{f_D} \rangle}{\mu \langle \overline{u} \rangle} = \alpha_0 + \alpha_1 \mathrm{Re}_p \quad (19)$$

as a function of plant Reynolds number

$$\mathrm{Re}_p = \frac{\langle \overline{u} \rangle d}{\nu} \quad (20)$$

where v is the kinematic viscosity of the fluid, $\langle \overline{u} \rangle$ is the fluid velocity averaged over the void space between stems, $\langle \overline{f_D} \rangle$ is the average drag (in the flow direction) per unit stem length. Eq. (19) assumes that α_0 varies with λ, and α_1 is a constant. It has been, however, experimentally shown that α_1 increases monotonically with λ and α_0 is approximately constant if $0.15 \le \lambda \le 0.35$. The vegetation layer provides an additional drag, which can be characterized by a drag coefficient (of Eq. (1)):

$$C_D \equiv \frac{\langle \overline{f_D} \rangle / \langle \bar{d} \rangle}{\frac{1}{2}\rho \langle \bar{u} \rangle^2} \quad (21)$$

using the average over a time interval much longer than representative time scales associated with turbulent fluctuations (denoted by an overbar) and using the space average over a void volume between plants (denoted by angular brackets). Substituting Eq. (19) in Eq. (21) yields a new form of the drag coefficient:

$$C_D = 2\left(\alpha_0 \mathrm{Re}_p^{-1} + 1\right) \quad (22)$$

of which the first term represents the viscous contributions, and the second term indicates the inertial contribution occurring due to the pressure loss in the cylinder wake. Previously, Koch and Ladd [64] investigated arrays of $\lambda = 0.05 - 0.4$ and observed that the cylinder drag can be characterized by a linear Re_p dependence similar to Eq. (19), but with both α_0 and α_1 varying with ϕ. White [61] also described the C_D of a smooth isolated cylinder for $1 < \mathrm{Re}_p < 10^5$ by an empirical expression:

$$C_D \approx 1 + 10.0\left(\mathrm{Re}_p\right)^{-2/3} \quad (23)$$

or equivalently

$$\frac{\langle \overline{f_D} \rangle}{\mu \langle \overline{u} \rangle} \approx 5.00\left(\mathrm{Re}_p\right)^{1/3} + \frac{1}{2}\mathrm{Re}_p \quad (24)$$

In Eq. (24), the second term is dominant relative to the first term based on the exponent of Re_p. It was observed that the inertial term α_1 increases monotonically with λ at a given Re_p, which is attributed in part to the spatial variance of the time-averaged longitudinal velocity which increases with λ. A linear regression of α_1 with λ yielded

$$\alpha_1 = (0.46 \pm 0.11) + (3.8 \pm 0.5)\lambda \quad (25)$$

as α_0 is also sensitive to the volume fraction λ [32,37,64]. Although Tanino et al. [37] discussed fundamental issues on the drag coefficient as proposed by Ergun's work [63] of Eq. (22), the data analysis indicates that α_0 is sensitive to both Re_p and λ.

3.2.2. Rominger and Nepf's work

Rominger and Nepf [57] investigated the interior flow within a rectangular porous zone consisting of embedded cylinders of various blockages, interpreted as an occupied volume fraction by the obstruction. The obstruction layer consists of a collection of uniformly sized rigid cylindrical plants, as shown in Fig. 1(c). The uniform rectangular configuration has a cylinder array in a 2D staggered lattice at half the distance between the nearest neighbor in both the x- and y-directions. Applying the shallow water equations for continuity in the stream-wise and cross-stream directions, the governing equations were set up as

$$\frac{\partial h\langle \overline{u} \rangle}{\partial x} + \frac{\partial h\langle \overline{v} \rangle}{\partial y} = 0 \quad (26)$$

$$\frac{\partial h\langle \overline{u} \rangle\langle \overline{u} \rangle}{\partial x} + \frac{\partial h\langle \overline{v} \rangle\langle \overline{u} \rangle}{\partial y} = -\frac{1}{\rho}\frac{\partial h\langle \overline{p} \rangle}{\partial x} + \frac{1}{\rho}\left[\frac{\partial h\langle \overline{p} \rangle}{\partial x} + \frac{\partial h\langle \overline{p} \rangle}{\partial y}\right] - hF_x \quad (27)$$

$$\frac{\partial h\langle \overline{u} \rangle\langle \overline{u} \rangle}{\partial x} + \frac{\partial h\langle \overline{v} \rangle\langle \overline{u} \rangle}{\partial y} = -\frac{1}{\rho}\frac{\partial h\langle \overline{p} \rangle}{\partial x} + \frac{1}{\rho}\left[\frac{\partial h\langle \overline{p} \rangle}{\partial x} + \frac{\partial h\langle \overline{p} \rangle}{\partial y}\right] - hF_y \quad (28)$$

where u and v are the fluid velocities in the x- and y-directions, respectively, p is the fluid pressure, and τ is the shear stress. The double average notation is used to denote the flow averaging within the rectangular configuration array within the macro time scale: $\langle \overline{u} \rangle$ indicates a time average of $\bar{u}$ that is the spatial average of u. $F_i (i = x, y)$ is the drag force exerted by the fluid, defined as,

$$F_x = \frac{1}{2}\frac{C_f}{H}\langle \overline{u} \rangle (\langle \overline{u} \rangle^2 + \langle \overline{v} \rangle^2)^{1/2} \quad (29)$$

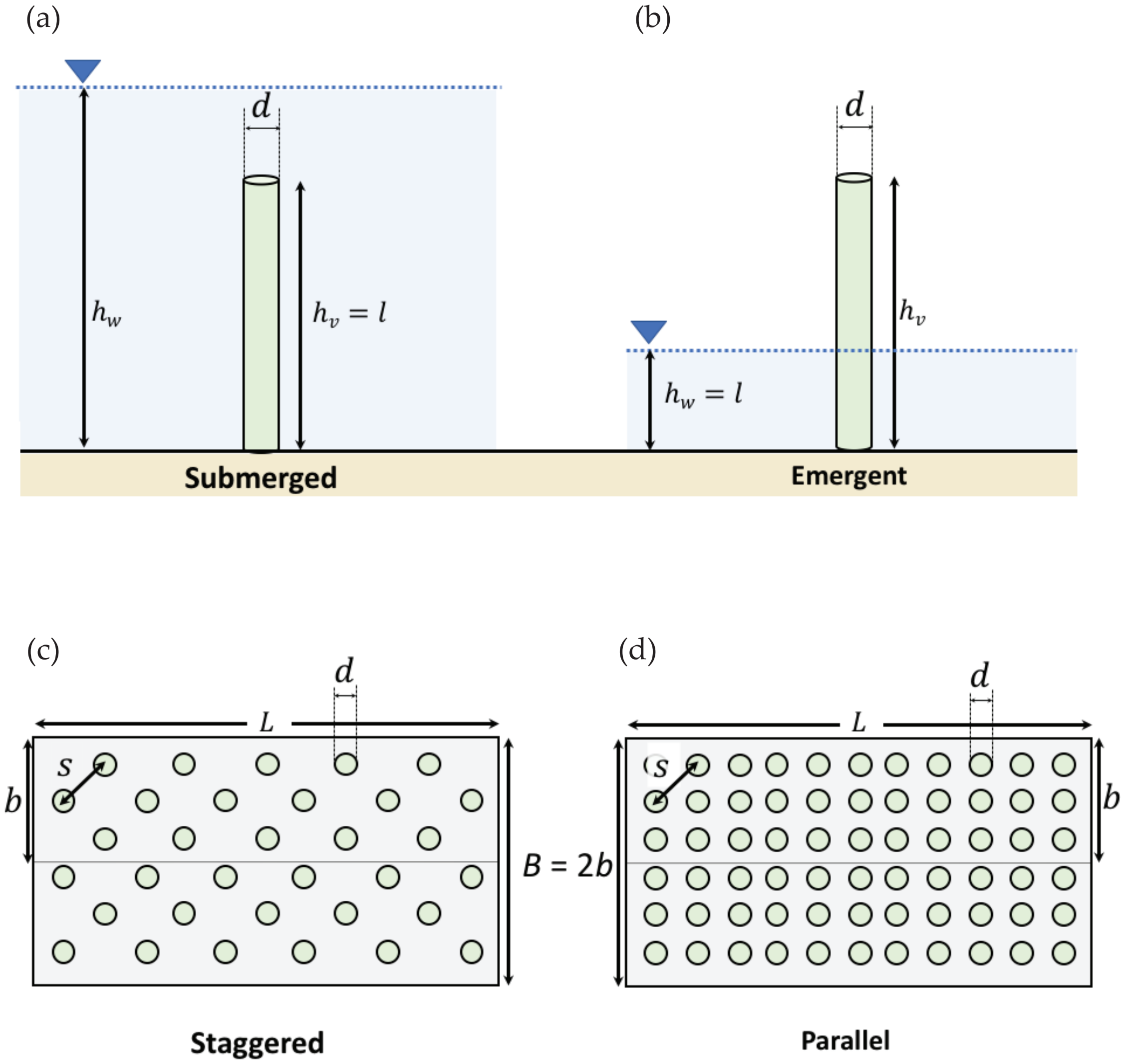

Fig. 1. Schematic of the geometric properties of an element representing a stem in (a) submerged, (b) emergent conditions, and top view of bioswale dimensions in (c) staggered and (d) parallel vegetation array patterns of length *L* and width *B* (=2*b*).

$$F_y = \frac{1}{2}\frac{C_f}{H}\langle\bar{v}\rangle\left(\langle\bar{u}\rangle^2 + \langle\bar{v}\rangle^2\right)^{1/2} \tag{30}$$

in which C_f represents the bed friction coefficient. The vertical length scale, H, is expressed as

$$H = \begin{cases} h_w & \text{outside the canopy} \\ (1-\phi)/a = \dfrac{1-\phi}{Nd} & \text{inside the canopy} \end{cases} \tag{31}$$

where $(1-\phi)/a$ indicates the void volume per projected area of the obstruction. The governing equations (Eqs. (27) and (28)) were scaled using the following characteristic parameters:

$$x \sim L,\quad y \sim b,\quad u \sim U_\infty,\quad v \sim \frac{bU_\infty}{L},\quad \frac{\partial u}{\partial x} \sim \frac{\Delta u}{L},\quad \text{and}\quad \frac{\partial p}{\partial x} \sim \frac{\Delta p}{L} \tag{32}$$

to have the following asymptotic relationships without the drag force terms

$$\rho\frac{U_\infty \Delta u}{L} \sim -\frac{\Delta p}{L} - \rho\frac{C_f}{2h(1-\phi)}U_\infty^2\left[1+\left(\frac{b}{L}\right)^2\right]^{1/2} \tag{33}$$

$$\rho\frac{U_\infty \Delta u}{L}\frac{b}{L} \sim -\frac{\Delta p}{b} - \rho\frac{C_f}{2h(1-\phi)}U_\infty^2\frac{b}{L}\left[1+\left(\frac{b}{L}\right)^2\right]^{1/2} \tag{34}$$

The pressure and inertial terms must be in a balance unconditionally only if $L \sim b$ for high flow-blockage. On the one hand, for a zero pressure gradient, the canopy length L is estimated as $(1-\phi)/C_D a$ and further simplified to $L \sim 2/C_D a$ for the low flow-blockage ($\phi \ll 1$) for $L \gg b$ as previously investigated by Belcher [65]. The length scale of the canopy at which the viscous and inertial forces are of the same order of magnitude was suggested as follows:

$$L = \left(5.5 \pm 0.4\right)\left[\left(\frac{2}{C_D a}\right)^2 + b^2\right]^{1/2} \tag{35}$$

where the coefficient 5.5 ± 0.4 was obtained experimentally. Eq. (35) indicates that the representative width b and length L of the canopy are correlated through the drag coefficient, C_D, while the viscous and inertial forces are balanced. To apply Eq. (35) to the bioswale design, the drag coefficient C_D needs to be represented using hydraulic parameters of runoff flows.

4. Application to bioswale design

4.1. Drag coefficient

Critical theories were closely reviewed in the previous section to determine specific BVL geometries. Within our approach, two conceptual equations are combined:

$$C_D = f\left(\mathrm{Re}_p\right) \tag{36}$$

such as Eqs. (22) and (23) and

$$C_D = f\left(\frac{L}{b}\right) \tag{37}$$

such as an inverse form of Eq. (35). Eqs. (36) and (37) can be interpreted as the hydraulic and geometric forms of the drag coefficient, C_D, respectively. For an emergent BVL, we re-write Eq. (35) as

$$C_D = \frac{2}{ab}\frac{1}{\sqrt{\eta^2 - 1}} \tag{38}$$

where

$$\eta = \frac{L}{5.5b} \tag{39}$$

is the dimensionless length scale, defined in this study. As noted earlier, 5.5 in Eq. (39) was empirically obtained in Rominger and Nepf's work [57]. In Eq. (38), the denominator ab (= Ndb) can be treated as a design parameter. An alternatively meaningful parameter can be a bed volume fraction, defined as follows:

$$\phi = \frac{\frac{\pi}{4}n_p d^2}{2bL} = \frac{\pi}{4}Nd^2 \tag{40}$$

where n_p is the number of stems within a BVL. Then, parameter ab has a specific expression of

$$ab = Ndb = \frac{4\phi}{\pi}\frac{b}{d} = \frac{2}{\pi}\phi\beta \tag{41}$$

where $\beta = 2b/d$ is a dimensionless width (i.e., the bioswale width divided by the stem diameter). Substitution of Eq. (41) into (38) gives

$$C_D = \frac{C_D^0}{\sqrt{\eta^2 - 1}} \tag{42}$$

where

$$C_D^0 = \frac{\pi}{\phi\beta} = \frac{2}{Nbd} \tag{43}$$

The drag coefficient decreases with volume fraction ϕ and the stem diameter d. For a long bioswale ($L \gg b$) of a bed volume fraction ϕ, the asymptotic behavior of the drag coefficient can be approximated as $C_D \propto 1/\left(L\phi\right)$. Here, we consider a specific exemplary case such that a stem has a volume fraction of ϕ ~ 0.314 and diameter 2.0 cm in a BVL of width $2b$ = 1.0 m, then we have

$$\beta = 1.0\,\mathrm{m} / 0.02\,\mathrm{m} = 50 \tag{44}$$

$$ab = \frac{2}{\pi}\phi\beta = \frac{2}{3.14} \times 0.314 \times 50 = 10 \tag{45}$$

$$C_D^0 = \frac{\pi}{\left(0.314\right) \times 50} = 0.02 \tag{46}$$

4.2. Graphical method

To easily estimate an optimized length ratio of a bioswale, we developed a graphical method as shown in Fig. 2. The drag coefficient C_D is plotted with respect to Re_p using Eq. (23) and η using Eq. (42). For example, if Re = $10^{14} \simeq 25.10$ (at position a), then C_D is calculated as 2.17 (at position b on the solid line). A horizontal line of C_D = 2.17 has nine cross-points with the same number of ab lines (from 0.1 to 20). Among them, we select two cases for ab = 0.2 and 2.0 (positions e and c,

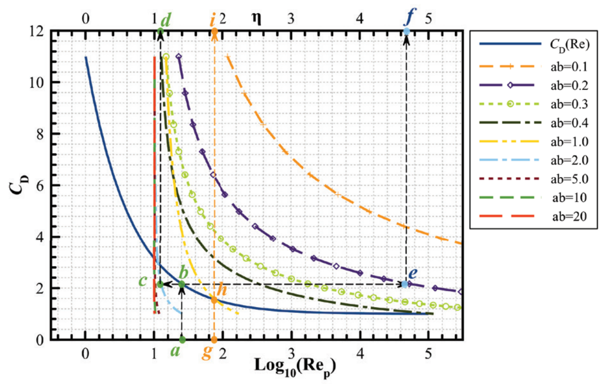

Fig. 2. Drag coefficient C_D plotted with respect to Re_p (bottom x-axis) and η (top x-axis) so as to find the optimal geometrical ratios for the bioswale design.

respectively) for an explanatory purpose. Position *d* was determined by drawing a vertical line at position *c*, which gives $\eta = 1.10$ and hence $L/2b = 3.03$. This result indicates that the representative BVL length of 3.03 m (if $2b = 1$ m) is required to approximately balance contributions from pressure and viscous forces. In other words, within the BVL of length 3.03 m, the inertial force is dominant over the viscous force. C_D rapidly approaches to 1.0 for $ab = 2$ within the reasonable range of Reynolds number, $10 < \mathrm{Re}_p \leq 100$, of the incoming flows. For $ab = 0.2$, position *e* provides a specific value of $\eta = 4.72$, which is equivalent to $L/2b$ ($=L/B$) = 13.0. This case indicates that for a BVL of width $B = 1$ m, the pressure and viscous forces are balanced near the end of the 13 m BVL. In summary, for a specific value of $\mathrm{Re}_p = 25.1$, the two cases of $ab = 2.0$ and 0.2 require the minimum lengths of 3.03 and 13.0 m, respectively, for the width $B = 1.0$ m. A bioswale of low density, narrow width, or smaller stem diameter requires a longer length for the hydraulic balance between the inertial and viscous forces. Position *h* (i.e., a cross position of $C_D = f(\mathrm{Re}_p)$ and that for $ab = 1.0$) gives a special case that log Re_p equals to η. A vertical line passing through the position *h* determines specific values of $\log_{10}(\mathrm{Re}_p)$ and η, which are 1.83 for both, and, hence, the length is estimated as $L = 4.40$ m per 1 m width BVL. As C_D is a rapidly decreasing function of log Re_p to 1.0, a matching point (similar to position *h*) must be located at a very high value of Re_p. In general, specific pair values of Re_p and η fully depend on the two functional representations of Eqs. (36) and (37). Basic mathematical dependence of C_D on Re_p is obtained by differentiating Eq. (23), which qualitatively gives

$$\frac{\partial C_D}{\partial \mathrm{Re}} < 0 \quad \text{and} \quad \frac{\partial C_D}{\partial \eta} < 0 \tag{47}$$

As Fig. 2 indicates, C_D unconditionally decreases with respect to Re_p and eventually converges to $C_D \to 1$ in the limit of $\mathrm{Re}_p \to \infty$. Variations of C_D with respect to L or η with a specific *ab* require significant elongation of the bioswale length at a high Reynolds number to decelerate the inter-stem flow enough. As we indicate this BVL length as the minimum, the designed BVL length can be a few factors longer than the minimum length estimated using the graphical method of Fig. 2. Differentiation of C_D with respect to the length L gives

$$\frac{\partial C_D}{\partial L} = -\frac{2}{abL}\frac{\eta^2}{\left[\eta^2 - 1\right]^{3/2}} \to -\frac{11}{aL} \tag{48}$$

which physically implies that for a long BVL (i.e., $\eta \gtrsim 3$ at least), the variation rate of C_D with L is insensitive to the half-width *b*.

4.3. Structure linked to hydraulics

Fig. 3 shows the geometrical ratio η plotted as a function of Re_p, through Eqs. (23) and (38), by eliminating evaluation of C_D. Note that this design relationship is applicable only to emergent conditions within specific ranges of $0.1 \leq ab \leq 20$ and $10^0 \leq \mathrm{Re}_p \leq 10^5$. Here, we select a slightly different value of $\mathrm{Re}_p = 10^{1.5} = 31.623$ (at position *j*) for a particular site; then, a vertical line is drawn that intersects with several crossing points of specific *ab* values. An exemplary case of $ab = 0.2$ is selected at position *k* from *j*. Then, position *l* was determined by drawing a horizontal line from *b*, which gives $\eta = 4.899$ and hence $L/B = 13.472$. For the BVL to be affective in decelerating flow, the length of the bioswale should be, in our opinion, three or more times the estimated L to ensure that the inertial force is dominant only near the inlet zone. Moreover, Fig. 3 shows interesting trends as follows. η rapidly increases with Re_p approximately for $ab \leq 1$. For cases of $ab \gtrsim 1$, η shows a very gradual increase in Re_p. In principle, one can eliminate C_D by equating Eqs. (23) and (42) to have

$$\eta = \sqrt{\left(\frac{\pi/\phi\beta}{1+10.0\mathrm{Re}_p^{-2/3}}\right)^2 - 1} = \sqrt{\left(\frac{2/ab}{1+10.0\mathrm{Re}_p^{-2/3}}\right)^2 - 1} \tag{49}$$

and asymptotically

$$\eta \simeq \frac{2/ab}{1+10.0\mathrm{Re}_p^{-2/3}} = \frac{2}{ab}\frac{\mathrm{Re}_p^{2/3}}{\mathrm{Re}_p^{2/3}+10.0} \tag{50}$$

or

$$L = \frac{11}{Nd}\frac{1}{1+10.0\mathrm{Re}_p^{-2/3}} \tag{51}$$

which indicates that a BVL length should be designed longer for low plant density N, smaller stem diameter d, and high runoff Reynolds number, Re_p. Then, Eq. (50) can be approximated for small and large Re_p such as

$$\eta \simeq \mathrm{Re}_p^{2/3}(5ab)^{-1} \quad \text{for} \quad \mathrm{Re}_p^{2/3} \ll 10.0 \tag{52}$$

$$\simeq 2(ab)^{-1} \quad \text{for} \quad \mathrm{Re}_p^{2/3} \gg 10.0 \tag{53}$$

The plateau values shown in Fig. 3 matches the limiting value of $\eta = 2/ab$ for high Re_p. For $\mathrm{Re}_p^{2/3} \ll 10.0$, the log η vs.

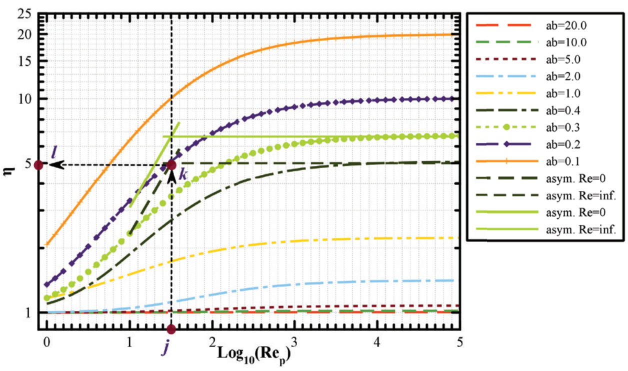

Fig. 3. η plotted with respect to Re_p determine optimized length ratio of a bioswale valid for $0.1 \leq ab \leq 20$ and $10^0 \leq \mathrm{Re}_p \leq 10^5$. Asymptotic lines drawn at zero and infinite Re_p are based on Eqs. (52) and (53), respectively.

log Re_p plot has a slope of 2/3. The boundary between the two limiting cases can be obtained by equating the two limiting η of Eq. (52), which gives the critical Reynolds number

$$Re_{p,cr} = 10^{1.5} = 31.623 \tag{54}$$

which is the exemplary case discussed earlier. Interestingly, this critical Reynolds number is universal and independent of *ab*. If the Reynolds number is higher than $Re_{p,cr}$, then one can simply use $\eta = 2/ab$ without losing design accuracy. Fig. 3 also shows the universal $Re_{p,cr}$ values by drawing asymptotic lines at zero and infinite Re_p for exemplary cases of $ab = 0.3$ and 0.4. The vertical line passing through position *k* re-emphasize the critical $Re_p = 31.623$, above which the variation of η with respect to Re_p becomes insensitive.

4.4. Verification and comparison

Fig. 4 shows a plot of Ishikawa et al.'s [66] experimental data onto η vs. Re_p graph. Ishikawa et al. [66] used a straight channel of fixed dimensions of 15 m × 0.3 m (or equivalently $\eta = 15\ \text{m}/(5.5 \times 0.15\ \text{m}) = 18.18$) to determine the effect of plant density on the drag force exerted onto the plants. We used their data set for two cases of the plant diameter $d = 6.4$ and 4.0 mm. In each case, they studied the drag coefficient for four plant densities, three bed slopes, and three discharge velocities. Ishikawa et al.'s [66] data, as summarized in Fig. 4, show a fixed η because a finite BVL size was used. Scattered data points grouped for a specific *ab* value indicate monotonously decreasing relationship between *ab* and Re_p. It is worth noting that variation of η is not sensitive to Re_p for each *ab* value. As predicted, η ranges approximately from 1.5 to 4.5 for *ab* values of Ishikawa's cases, and ratio η_{ex}/η_{thr} ranges roughly from 4 to 12, where η_{ex} and η_{thr} are experimental and theoretical η, respectively. This η range ensures that the inertial force is dominant only near the inlet canopy region.

4.4.1. Safety factor

As our predicted value of η indicates the proper BVL length at which the pressure and viscous forces are in balance with each other, the dimensionless length range from η to 2η can be interpreted as a BVL zone so that the inertial force becomes less significant than the viscous force. Moreover, in the range of the dimensionless length longer than 2η, the viscous force becomes dominant so that the BVL provides an effective hydraulic resistance to decelerate the entered runoff flow at the inlet of the canopy zone. We suggest a safety factor of 3–5 to be multiplied to the theoretical η obtained using the graphical method to ensure that the BVL zone effectively provides hydraulic resistance to decelerate the incoming runoff flows.

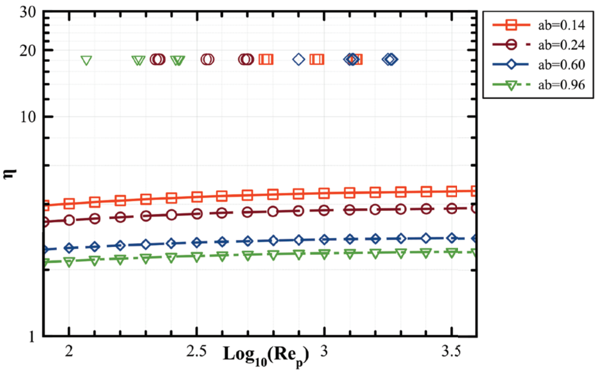

Fig. 4. Comparison of experimental data from Ishikawa's study [66] (η = 18.18) with the plot η vs. Re_p.

5. Concluding remarks

Flow resistance and channel-conveyance capacity are basic design parameters required in the hydraulic design of a vegetated bioswale layer. Current design for bioswales include five methods such as Darcy's law, rational method, Manning's equation, curve number method, and first-flush sizing method. To support the widespread adoption of bioswales, there is a need for improved techniques regarding the predictive capability of hydraulic drag within and above the BVL so as to optimize design methods. This study provides an original contribution to the literature involving the coupling of structural and hydraulic aspects of bioswale systems.

After the in-depth review of canopy-flow theories, we employed Rominger and Nepf's [57] and Baptist's [60] work to directly link plant Reynolds number and length scales of the bioswale systems by mathematically eliminating C_D. We then predicted a theoretical minimum length so as to balance the pressure and viscous forces near the outlet of the bioswale. These formulas can be unified in a general form of an emergent case that links the plant Reynolds number and η (= $L/2.75B$) as a structural design parameter. We suggest a proper length of a vegetated bioswale to be calculated as at least 3–5 times the theoretically predicted η using the graphical method developed in this study. Engineers can draw upon this method as a tool that can provide them with guidance regarding the predictive capability in the proper BVL length so as to enhance bioswale operation and maintenance.

Acknowledgments

This work was supported by the Kohala Center of Hawaiian Scholars Doctoral Fellowship Program (formerly known as the Mellon-Hawai'i Doctoral and Postdoctoral Fellowship Program), the Deviants from the Norm Fund and Dr. Paul and Elizabeth Nakayama for the first author.

Symbols

$\langle \bar{d} \rangle$	—	Characteristic plant width
$\hat{h}_w$	—	Scaled length of water depth
$\hat{l}$	—	Wetted stem height per water height
$\hat{s}$	—	Scaled length of average vegetation height
$\langle \overline{f_D} \rangle$	—	Average drag in the direction of the average flow per unit length of stem
$\langle \bar{u} \rangle$	—	Fluid velocity averaged over the void space between stems
$\bar{u}$	—	Depth-averaged flow velocity
a	—	Projected plant area per volume, Nd_s
A_c	—	Front cross-sectional area
B	—	Width of a vegetation layer

b	—	Half width of a vegetation layer
C_b	—	Chézy coefficient of the bed
C'_b	—	Drag force for both submerged and emergent vegetation conditions
C_D	—	Drag coefficient
C_f	—	Bed friction coefficient
d_s	—	Stem diameter
f	—	Stress ratio
F_D	—	Average drag force
f_b	—	Friction factor
F_i	—	Drag force exerted on the fluid in the x- and y-directions for ($i = x, y$)
g	—	Gravitational acceleration
H	—	Vertical length scale of the canopy
h_{onset}	—	Water height of resistance onset
h_v	—	Physical vegetation height
h_w	—	Dynamic water height
L	—	Length of a vegetation layer
l	—	Wetted vegetation height
N	—	Number of plants per unit plant area
R	—	Flow resistance
r	—	Hydraulic radius
S	—	Channel slope
s	—	Spacing between stems
u	—	Fluid velocity in the x-direction
u_*	—	Frictional velocity
U_∞	—	Uniform flow
u_{rms}	—	Vertical turbulent intensity in the stream-wise direction
U_h	—	Slip velocity on the top of the obstruction layer
V	—	Mean flow velocity averaged over the void space
v	—	Fluid velocity in the y-direction
V_c	—	Maximum velocity within the vegetation layer
V_l	—	Approaching velocity
Re_p	—	Plant Reynolds number

Greeks

α_0, α_1	—	Empirical coefficients
δ_e	—	Length scale of the vertical flow penetration
κ	—	Von Karman's constant
λ	—	Fraction of the bed area occupied by cylindrical stems
v	—	Kinematic viscosity
ω_{rms}	—	Vertical turbulent intensity at the interface
ϕ	—	Solid volume fraction
ρ	—	Density of water
τ	—	Stress

Subscripts

BTH	—	Barfield, Tollner, and Hayes
B	—	Baptist
Ch	—	Cheng
SS	—	Stone and Shen
B	—	Bed
v	—	Vegetation
w	—	Water

References

[1] Prince George's County Department of Environmental Protection, Design Manual for Use of Bioretention in Stormwater Management, Technical Report, 1993.
[2] Prince George's County Maryland, Bioretention manual, Tech. Rep., Environmental Services Division, Department of Environmental Resources, 2007.
[3] Prince George's County, Stormwater Management Design Manual, Tech. Report, 2014.
[4] USEPA, Storm Water Technology Fact Sheet - Wet Detention Ponds, Tech. Rep. EPA 832-F-99-048, 1999.
[5] M.E. Dietz, Low impact development practices: a review of current research and recommendations for future directions, Water Air Soil Pollut., 186 (2007) 351–363.
[6] M.E. Dietz, J.C. Clausen, Stormwater runoff and export changes with development in a traditional and low impact subdivision, J. Environ. Manage., 87 (2008) 560–566.
[7] Q. Xiao, E. McPherson, Q. Zhang, X. Ge, R. Dahlgren, Performance of two bioswales on urban runoff management, Infrastructures, 2 (2017) 12.
[8] R.A. Purvis, R.J. Winston, W.F. Hunt, B. Lipscomb, K. Narayanaswamy, A. McDaniel, M.S. Lauffer, S. Libes, Evaluating the water quality benefits of a bioswale in Brunswick County, North Carolina (NC), USA, Water, 10 (2018) 1–16.
[9] J. Irvine, A. Kim, Understanding bioswale as a small water and wastewater treatment plant: a theoretical review, Desal. Wat. Treat., 135 (2018) 1–15.
[10] W.F. Hunt, B. Lord, B. Loh, A. Sia, Plant Selection for Bioretention Systems and Stormwater Treatment Practices, Springer, New York, 2015.
[11] M. Bäckström, Sediment transport in grassed swales during simulated runoff events, Water Sci. Technol. 45 (2002) 41–49.
[12] M. Bäckström, Grassed swales for stormwater pollution control during rain and snowmelt, Water Sci. Technol. 48 (2003) 123–132.
[13] S. Achleitner, C. Engelhard, U. Stegner, W. Rauch, Local infiltration devices at parking sites - Experimental assessment of temporal changes in hydraulic and contaminant removal capacity, Water Sci. Technol. 55 (4) (2007) 193–200.
[14] G. Roinas, C. Mant, J. B. Williams, Fate of hydrocarbon pollutants in source and non-source control sustainable drainage systems, Water Sci. Technol. 69 (2014) 703–709.
[15] Q. Xiao, E. G. McPherson, Performance of engineered soil and trees in a parking lot bioswale, Urban Water J. 8 (4) (2011) 241–253.
[16] S. A. Trowsdale, R. Simcock, Urban stormwater treatment using bioretention, J. Hydrology 397 (2011) 167–174.
[17] J. Li, C. Jiang, T. Lei, Y. Li, Experimental study and simulation of water quality purification of urban surface runoff using non-vegetated bioswales, Ecol. Eng. 95 (2016) 706–713.
[18] S. M. Charlesworth, E. Nnadi, O. Oyelola, J. Bennett, F. Warwick, R. Jackson, D. Lawson, Laboratory based experiments to assess the use of green and food based compost to improve water quality in a Sustainable Drainage (SUDS) device such as a swale, Sci. Total Environ. 424 (2012) 337–343.
[19] J. Li, Y. Li, J. Zhang, Y. Li, Bioswale column experiments and simulation of pollutant removal from urban road stormwater runoff, Desal. Water Treat. 57 (2016) 24894–24912.
[20] Hawaii Office of Planning, Low impact development a practitioner's guide LID Hawaii, Tech. rep., Coastal Zone Management Program, National Oceanic and Atmospheric Administration, 2006.
[21] Las Vegas Stormwater Quality Management Committee, Las Vegas Valley construction site best management practices guidance manual, Tech. report, 2009.
[22] Alaska Department of Environmental Conservation, Alaska storm water guide, Tech. report, 2011.
[23] Arizona Department of Transportation, Erosion and Pollution Control Manual for Highway Design and Construction, Tech. report, 2012.
[24] California Stormwater Quality Association, Stormwater Best Management Practice Handbook: New Development and Redevelopment, Tech. report, 2003.

[25] A. Roy-poirier, P. Champagne, A.M. Asce, Y. Filion, Review of bioretention system research and design: past, present, and future, J. Environ. Eng., 136 (2010) 878–889.
[26] New Mexico State Highway and Transportation Department, Drainage Manual Volume 1, Hydrology, Tech. report, 1995.
[27] City and County of Honolulu, Storm water BMP Design Guide for New and Redevelopment, Tech. report, 2017.
[28] Utah Department of Transportation, Stormwater Quality Design Manual, Tech. report, 2018.
[29] Washington State Department of Ecology Water Quality, Stormwater Management Manual for Western Washington, Tech. report, 2012.
[30] State of Oregon Department of Environmental Quality, Biofilters (Bioswales, Vegetative Buffers, and Constructed Wetlands) for Storm Water Discharge Pollution Removal, Tech. report, Department of Environmental Quality, 2003.
[31] Idaho Department of Environmental Quality, Catalog of Stormwater Best Management Practices for Idaho Cities and Counties, Tech. report, 2005.
[32] S. Petryk, Drag on Cylinders in Open Channel Flow, Ph.D. Thesis, Colorado State University, 1969.
[33] J.J. Finnigan, P.J. Mulhearn, A simple mathematical model of airflow in waving plant canopies, Boundary-Layer Meteorol., 14 (1978) 415–431.
[34] J.J. Finnigan, Turbulent Transport in Flexible Plant Canopies, The Forest-Atmosphere Interaction, 1985, pp. 443–480
[35] J.J. Finnigan, Y. Brunet, Turbulent Airflow in Forests on Flat and Hilly Terrain, in: Wind and trees, Cambridge University Press, New York, 1995, pp. 3–40.
[36] B.M. Stone, H.T. Shen, Hydraulic resistance of flow in channels with cylindrical roughness, J. Hydraul. Eng., 128 (2002) 500–506.
[37] Y. Tanino, Y. Tanino, H.M. Nepf, H.M. Nepf, Laboratory investigation of mean drag in a random array of rigid, emergent cylinders, J. Hydraul. Eng., 134 (2008) 34–41.
[38] A. Vargas-Luna, A. Crosato, W.S. Uijttewaal, Effects of vegetation on flow and sediment transport: Comparative analyses and validation of predicting models, Earth Surface Process. Landforms, 40 (2015) 157–176.
[39] N. Fathi-Maghadam, M. Kouwen, Nonrigid, non-submerged, vegetative roughness on floodplains, J. Hydraul. Eng., 8 (1997) 51–57.
[40] J. Finnigan, Turbulence in plant canopies, Annu. Rev. Fluid Mech., 32 (2000) 519–571.
[41] A. Espinosa-Gayosso, M. Ghisalberti, G.N. Ivey, N.L. Jones, Particle capture and low-Reynolds-number flow around a circular cylinder, J. Fluid Mech., 710 (2012) 362–378.
[42] A. Espinosa-Gayosso, M. Ghisalberti, G.N. Ivey, N.L. Jones, Particle capture by a circular cylinder in the vortex-shedding regime, J. Fluid Mech., 733 (2013) 171–188.
[43] A. Espinosa-Gayosso, M. Ghisalberti, G.N. Ivey, N.L. Jones, Density-ratio effects on the capture of suspended particles in aquatic systems, J. Fluid Mech., 783 (2015) 191–210.
[44] A.T. King, R.O. Tinoco, E.A. Cowen, A k-ϵ turbulence model based on the scales of vertical shear and stem wakes valid for emergent and submerged vegetated flows, J. Fluid Mech., 701 (2012) 1–39.
[45] M. Gao, W. Huai, Y. Xiao, Z. Yang, B. Ji, Large eddy simulation of a vertical buoyant jet in a vegetated channel, Int. J. Heat Fluid Flow, 70 (2018) 114–124.
[46] M. Jamali, X. Zhang, H.M. Nepf, Exchange flow between a canopy and open water, J. Fluid Mech., 611 (2008) 237–254.
[47] X. Zhang, H.M. Nepf, Thermally driven exchange flow between open water and an aquatic canopy, J. Fluid Mech., 632 (2009) 227–243.
[48] F. Huthoff, Modeling hydraulic resistance of floodplain vegetation, Fredrik Huthoff, Enschede, the Netherlands, 2007.
[49] W. Yang, S.U. Choi, A two-layer approach for depth-limited open-channel flows with submerged vegetation, J. Hydraul. Res., 48 (2010) 466–475.
[50] N.S. Cheng, Representative roughness height of submerged vegetation, Water Resour. Res., 47 (2011) 1–18.
[51] Y. Ishikawa, T. Sakamoto, K. Mizuhara, Effect of density of riparian vegetation on effective tractive force, J. Forest Res., 8 (2003) 235–246.
[52] S. Petryk, G. Bosmajian, Analysis of Flow through Vegetation, J. Hydraul. Div., 101 (1975) 871–884.
[53] R. Raupach, Drag and drag partition on rough surfaces, Boundary-Layer Meteorol., 60 (1992) 375–395.
[54] C.S. James, A.L. Birkhead, A.A. Jordanova, J.J. O'Sullivan, Flow resistance of emergent vegetation, J. Hydraul. Res., 42 (2004) 390–398.
[55] R.G. Sharpe, C.S. James, Deposition of sediment from suspension in emergent vegetation, Water SA, 32 (2006) 211–218.
[56] U.C. Kothyari, H. Hashimoto, K. Hayashi, Effect of tall vegetation on sediment transport by channel flows, J. Hydraul. Res., 47 (2009) 700–710.
[57] J.T. Rominger, H.M. Nepf, Flow adjustment and interior flow associated with a rectangular porous obstruction, J. Fluid Mech., 680 (2011) 636–659.
[58] B. Barfield, E. Tollner, J. Hayes, Filtration of sediment by simulated vegetation II. Unsteady flow with non-homogeneous sediment, Trans. Am. Soc. Agric. Eng., 22 (1979) 1063–1067.
[59] C. Herschel, On the origin of the Chézy formula, J. Assoc. Eng. Soc., 18 (1859) 363–370.
[60] M.J. Baptist, Modelling Floodplain Biogeomorphology, Ph.D. Thesis, Delft University of Technology, 2005.
[61] F.M. White, Viscous Fluid Flow, 2nd ed., McGraw-Hill, New York, 1991.
[62] M. Ghisalberti, Obstructed shear flows: Similarities across systems and scales, J. Fluid Mech., 641 (2009) 51–61.
[63] S. Ergun, Fluid flow through packed columns, Chem. Eng. Sci., 48 (1952) 89–94.
[64] D.L. Koch, A.J.C. Ladd, Moderate Reynolds number flows through periodic and random arrays of aligned cylinders, J. Fluid Mech., 349 (1997) 31–66.
[65] S.E. Belcher, N. Jerram, J.C.R. Hunt, Adjustment of a turbulent boundary layer to a canopy of roughness elements, J. Fluid Mech., 488 (2003) 369–398.
[66] Y. Ishikawa, K. Mizuhara, S. Ashida, Effect of density of tress on drag exerted on trees in river channels, J. Forest Res., 5 (2000) 271–279.